THE UNIVERSITY OF MICHIGAN

INDUSTRY PROGRAM OF THE COLLEGE OF ENGINEERING

VOID FRACTION MEASUREMENTS IN CAVITATING MERCURY

Frederick G. Hammitt
Willy Smith
Ian E. B. Lauchlan
Richard D. Ivany
M. John Robinson

March, 1964

IP-661

TABLE OF CONTENTS

Page

LIST OF FIGURES..... iii

I INTRODUCTION..... 1

II DESCRIPTION OF EQUIPMENT..... 2

III EXPERIMENTAL PROCEDURE..... 7

A Axial Alignment and Centerline Determination..... 7

1 Optical Alignment Determination..... 7
2 Centerline Determination by Symmetry..... 9

B Cavitation and Flow Conditions..... 9

IV TEST RUNS..... 11

V THEORETICAL ANALYSIS AND DATA REDUCTION..... 13

VI DISCUSSION OF RESULTS..... 18

A Local Density Measurements..... 18
B Centerline Plane Mean Density Measurements..... 19
C Central Jet Axial Density Profiles..... 28

VII CONCLUSIONS..... 29

VIII APPENDIX..... 29

ACKNOWLEDGMENTS..... 31

REFERENCES AND FOOTNOTES..... 32

LIST OF FIGURES

Figure		Page
1	Overall Loop Layout.....	3
2	Cross Section of Cavitating Venturi Test Section Showing Locations of Metal Wear Specimens and Locations of the Cavitation Termination for Various Degrees of Cavitation.....	4
3	Cross Section of Densitometer.....	5
4	Densitometer Positioned at Venturi.....	6
5	Block Diagram of Electronic Equipment.....	8
6	Determination of Venturi Centerline by Densitometer Method, Assuming Axial Symmetry.....	10
7	Void Fraction Profiles for Standard and First Mark Cavitation Conditions.....	12
8	Count-rate vs. Axial Position for Standard Cavitation at 34 ft./sec. Throat Velocity.....	14
9	Count-rate vs. Axial Position for First Mark Cavitation at 34 ft/sec Throat Velocity.....	15
10	Calculation of $\rho(r)$ from $\rho(x)$.....	17
11	Normalized Fluid Density vs. Axial Position for Visible Initiation at 34 ft./sec. Throat Velocity....	20
12	Normalized Fluid Density and Core Void Fraction vs. Axial Position for Cavitation to Nose at 34 ft./sec. Throat Velocity.....	21
13	Normalized Fluid Density and Core Void Fraction vs. Axial Position for Standard Cavitation at 34 ft./sec. Throat Velocity.....	22
14	Normalized Fluid Density vs. Axial Position for Cavitation to Back at 34 ft./sec. Throat Velocity....	23
15	Normalized Fluid Density and Core Void Fraction vs. Axial Position for First Mark Cavitation at 34 ft./sec. Throat Velocity.....	24

LIST OF FIGURES (CONT'D)

Figure		Page
16	Normalized Fluid Density vs. Axial Position for Cavitation to Nose at 48 and 34 ft./sec. Throat Velocities.....	25
17	Normalized Fluid Density vs. Axial Position for Standard Cavitation at 48 and 34 ft./sec. Throat Velocities.....	26
18	Void Fraction Contour Schematic.....	29

I INTRODUCTION

Two-phase flow in mercury and other liquid metals at elevated temperature has acheived substantial technological importance in recent years in connection with SNAP-type powerplants using liquid metal Rankine cycles. In such systems, two-phase flow is required in the boiler and condenser. It may also exist in pumping units, valves, etc., in a less desirable form as cavitation, affecting fluid-dynamic performance unfavorably and causing rapid pitting of exposed components. For the quantitative study of these two-phase phenomena, void fraction (or density) measurements are necessary. A gamma-ray densitometer is at present the most feasible instrument available for the purpose.

The present paper describes the development and use of such an instrument, using Co^{60}, for density measurements in cavitating mercury in a venturi. A high-energy gamma, such as that from Co^{60}, generally becomes desirable for a dense medium such as mercury, while much softer radiation (as provided by Tm^{170} or a promethium-tungstate target source) is desirable for low density fluids as water or alkali liquid metals, e.g.

The present measurements have been of two types:

1) Local density determination, i.e., a function of radius and axial position in an axially-symmetric flow, and

2) Mean density determination in a plane including the centerline as a function of axial position.

The first set of measurements have been previously reported,[1] whereas the second set[2] is new. The two sets of data in combination are used to supply additional basic detailed information regarding the local structure

of the flow, while the new data alone are to be used as an indication of the extent of the cavitating region.

Thus, it is believed that the work herein discussed is useful both in terms of the further development of a technique useful over a broad range of research investigations, and in terms of the acquisition of new basic data applicable to an important flow situation in a particular case.

II DESCRIPTION OF EQUIPMENT

The gamma-ray densitometer and the general technique have been previously described.[1] For convenience the most significant portions will be summarized here. Figure 1 is a schematic of the mercury tunnel facility used and Figure 2 is a cross-section drawing of the cavitating plexiglas venturi test section. During some of the runs two "wear specimens" (Figure 2) were in place. Figure 3 is a schematic cross-section drawing of the densitometer, showing the proper relation of source, collimators, venturi, detector, and shielding; and Figure 4 is a photograph of the overall densitometer-venturi assembly.

The collimators have rectangular appertures, 0.030 by 0.200 in., accurately aligned; the longer dimension being parallel to the direction of flow. The change in flow conditions in the axial direction over the length of the aperature is small compared to that in the radial direction. The transverse (radial) 0.030 in. dimension is small enough to detect significant variations with position. In combination with the 0.200 in. axial dimension, it allows the passage of enough gammas to give a statistical accuracy of about 1 percent with the 20 milli-curie Co^{60} source used.

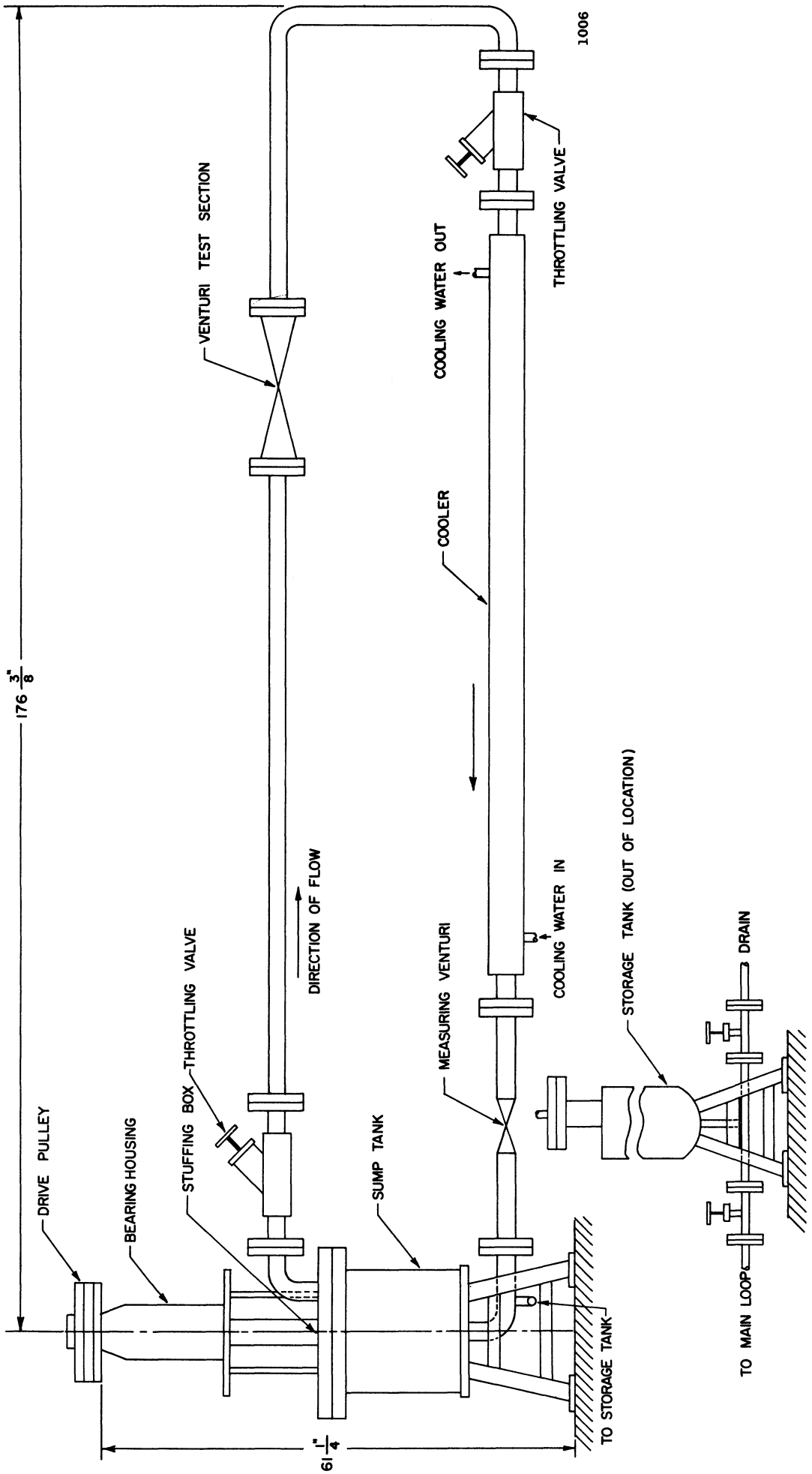

Figure 1. Overall Loop Layout.

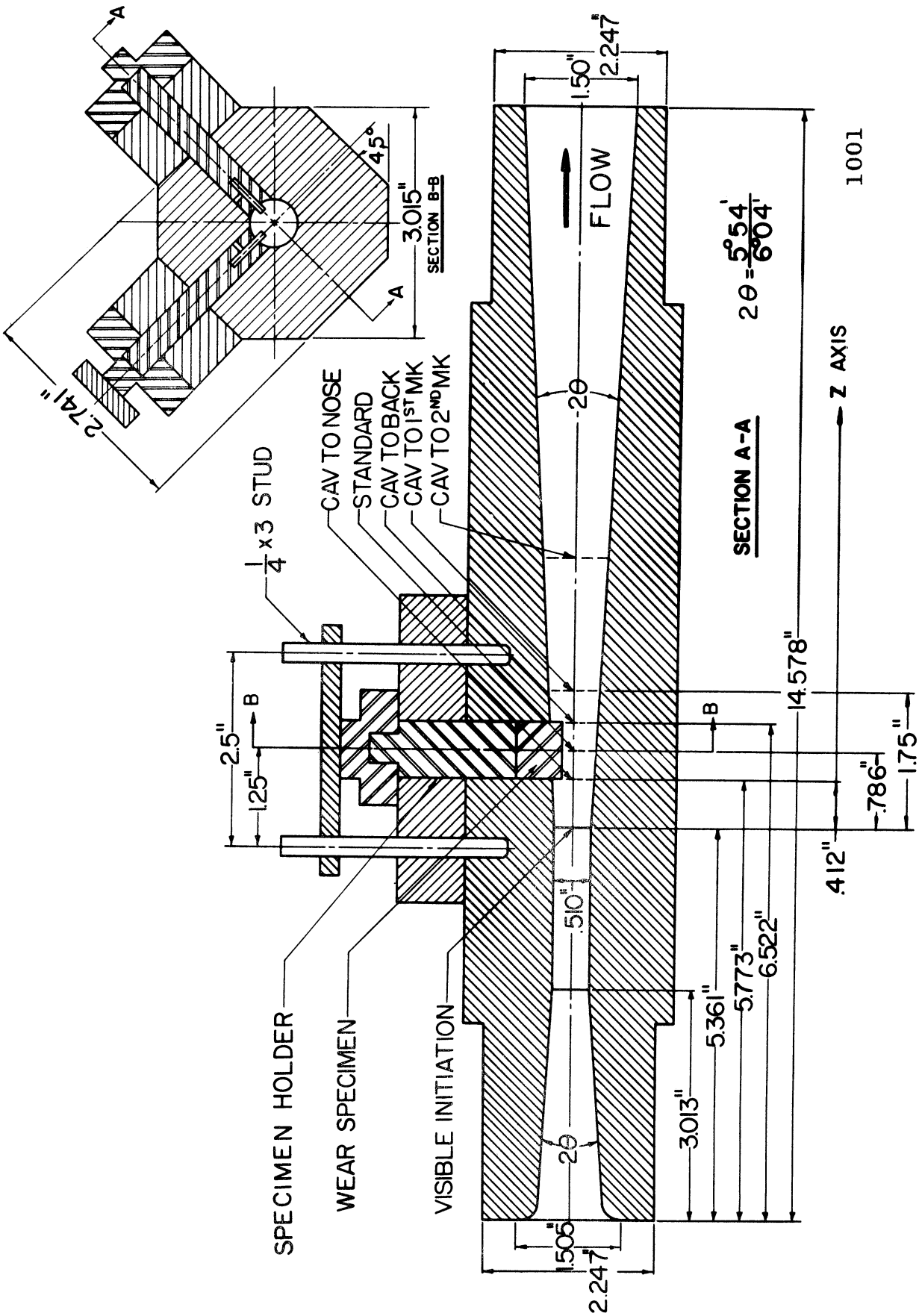

Figure 2. Cross Section of Cavitating Venturi Test Section Showing Locations of Metal Wear Specimens and Locations of the Cavitation Termination for Various Degrees of Cavitation.

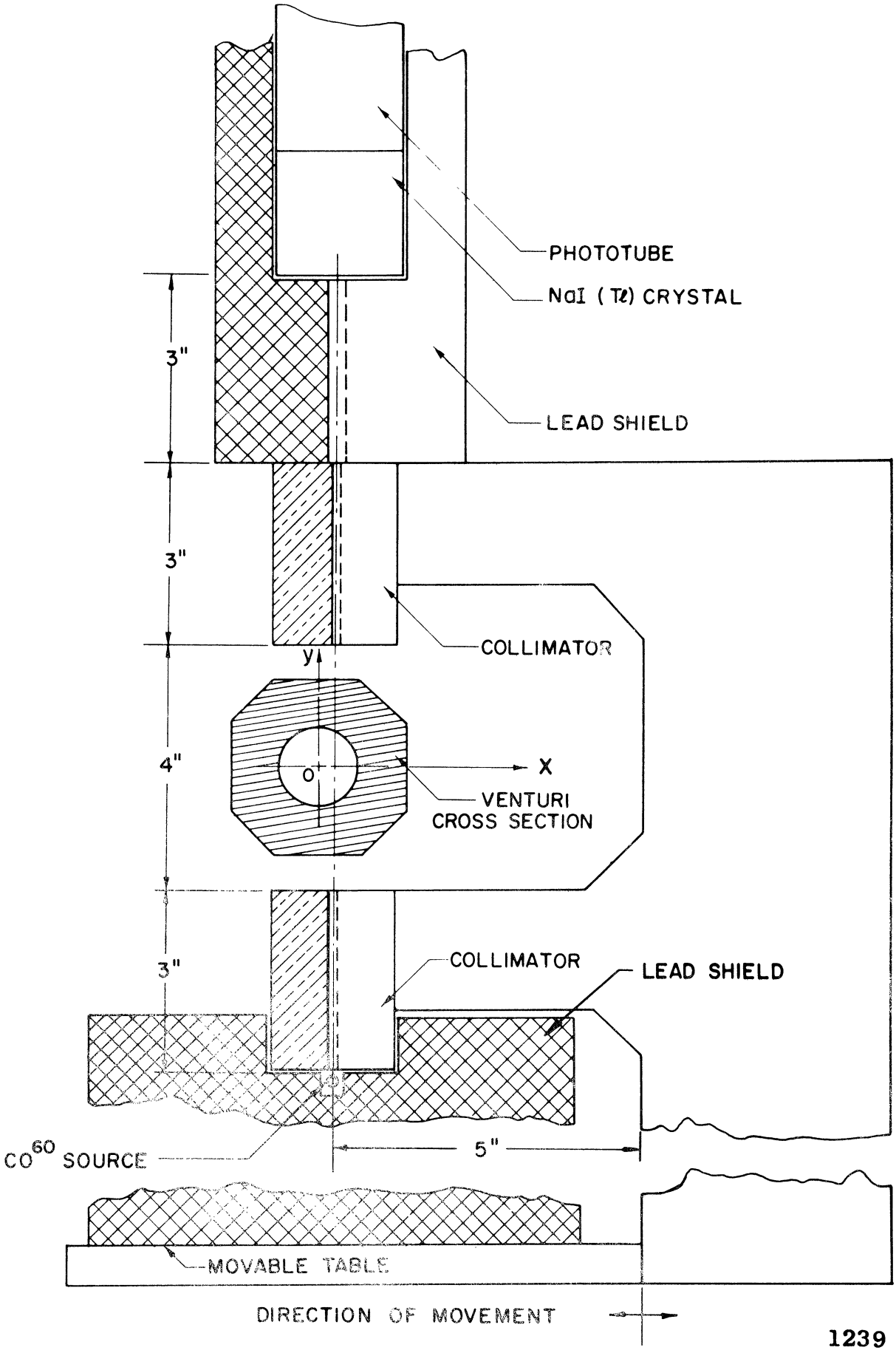

Figure 3. Cross Section of Densitometer.

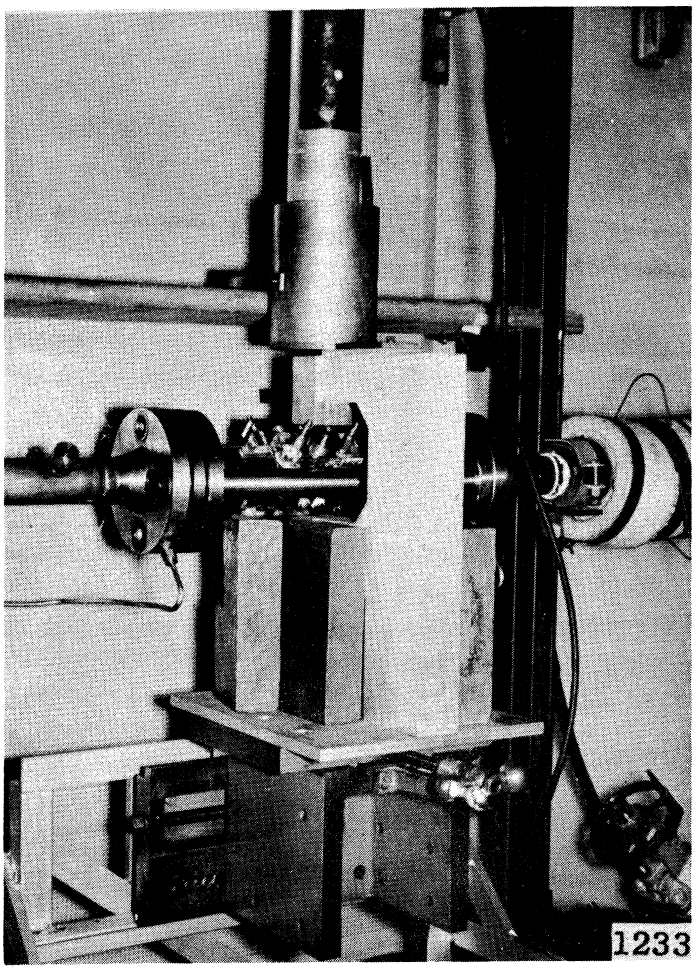

Figure 4. Densitometer Positioned at Venturi.

Obviously the selection of collimator design, and source type and strength, represents a compromise between the requirements of handling ease and safety, precision of location, counting statistics, significant flow parameters, and type of fluid. A change of any of these factors would of course alter the optimum design.

The whole assembly is mounted on a cross-compound index talbe (Figure 4) so that horizontal movement of the vertical gamma-ray beam in the radial and axial directions is possible to about ± 0.003 in. accuracy. Lead brick shielding is used for personnel protection.

Figure 5 is a block diagram of the electronic circuitry which is as previously described.(1) A single-channel analyzer permits the separation of the 1.17 Mev peak from the entire pulse height spectrum, so that only the effect of an unscattered single-energy photon need be considered in the calculations.

III EXPERIMENTAL PROCEDURE

A. Axial Alignment and Centerline Determination

The location of the venturi centerline relative to the collimator was determined by two independent procedures which were found to agree closely.

1. Optical Alignment Determination

The top and bottom collimators were aligned with respect to each other by placing a light source in the scintillation-tube holder, and moving the bottom collimator within the adjustment provided, so that a maximum light intensity would pass through the slit.

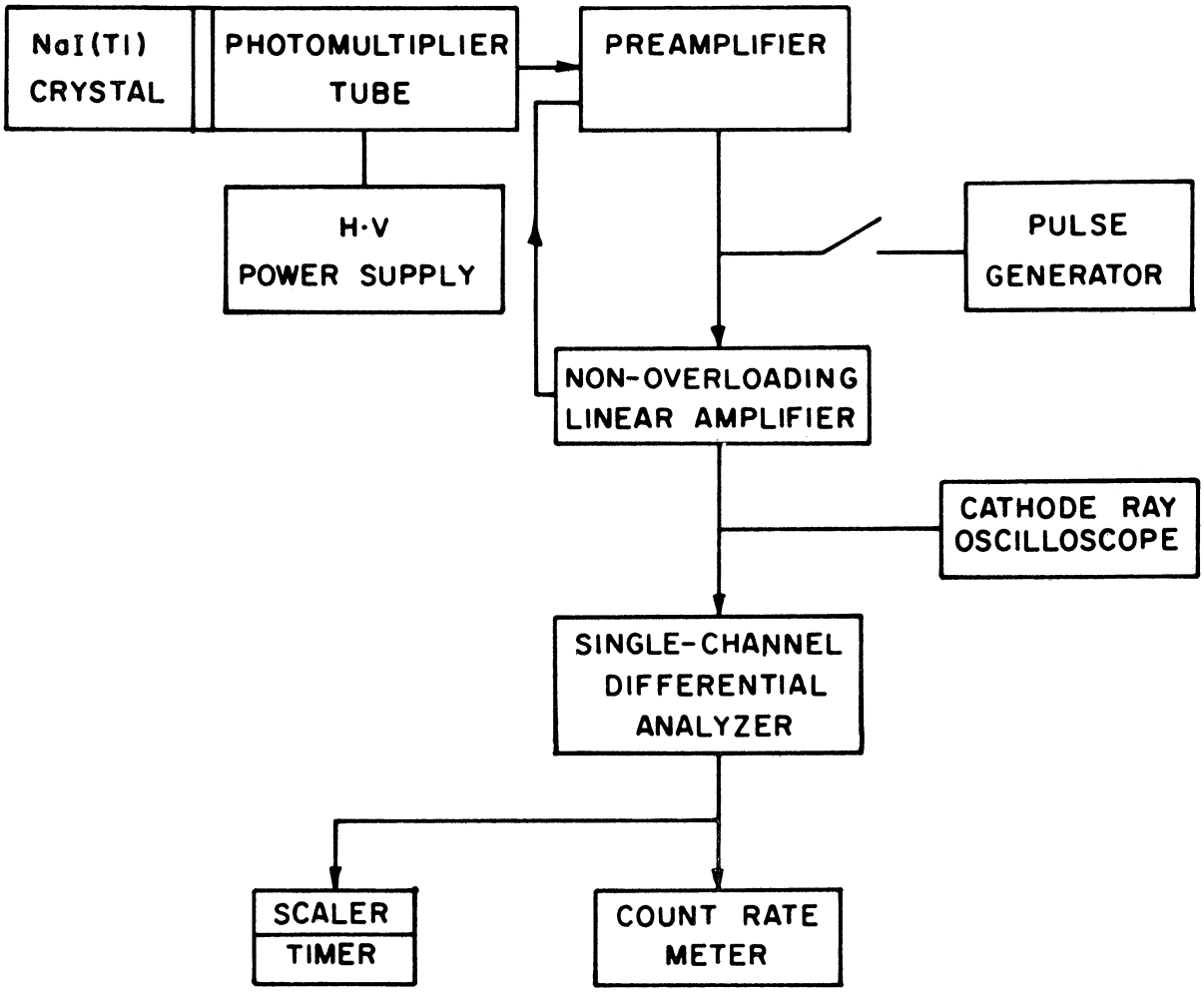

Figure 5. Block Diagram of Electronic Equipment.

The plexiglas venturi was then placed in position and rotated so that its flat outer surfaces were parallel to the surfaces of the collimators (noting that the light beam would be refracted unless this were the case). The table was then moved in the cross-wise direction until the light beam passed through both collimators. This could only occur, considering that the outer faces of the venturi were normal to the beam, when the internal surfaces were also normal to the beam, and hence the light not refracted. Thus the venturi centerline was located at a given axial position in terms of a known setting for the planing table cross-feed adjustment. Minor adjustments of the planing table position were made until it was possible to traverse the collimator assembly in the axial direction without deviating from the venturi centerline.

2. Centerline Determination by Symmetry

With the loop filled with mercury and the Co^{60} source in place, a series of count-rate measurements were made at 0.05 inch traverse intervals across the venturi. Assuming axial symmetry, the centerline coincides with the minimum in the count-rate curve (Figure 6), and it is seen that this minimum is located at the centerline as previously determined.

Since the results of these two independent methods of alignment and centerline determination were essentially the same, it is felt that the location of the true venturi centerline has been established with satisfactory precision.

B. Cavitation and Flow Conditions

In the mercury cavitation tests using a given venturi design (Figure 2), there are essentially two independent variables:

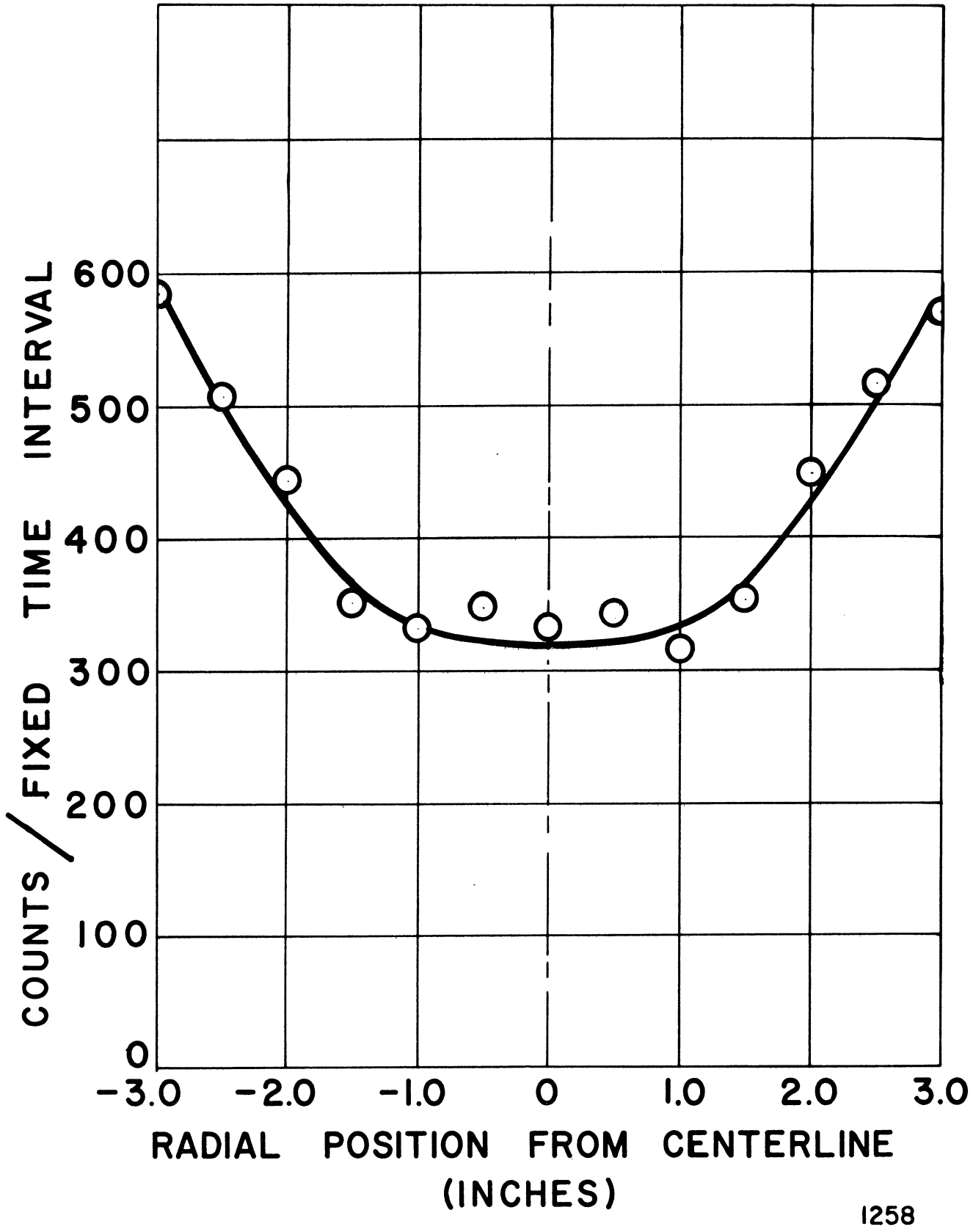

Figure 6. Determination of Venturi Centerline by Densitometer Method, Assuming Axial Symmetry.

1) Throat velocity

2) Extent of cavitating region ("degree of cavitation")

The relationships between these and the other parameters of interest such as cavitation number, pressure, temperature, fluid, gas content, etc., are complex, have been discussed in various other papers and reports from other investigations and from the present investigation[3] e.g., and will not be treated in this paper. However, for a given setting of these two independent variables, one of the bits of basic information necessary to attain a fuller understanding of the overall phenomenon is the local density (or "void fraction"). Also, a measurement of this quantity, or more simply, of the mean density at a given axial position in a plane including the venturi centerline is most desirable to assist in setting the "degree of cavitation" for those cases where visual observation is not possible, e.g., in a test with high-temperature liquid metals. The various "degrees of cavitation" are shown in Figure 2 where the termination points of the cavitating region are marked.

IV TEST RUNS

A set of test runs was made previously,[1] wherein both radial and longitudinal traverses were made. Local density measurements, as a function of radius and axial position, were attained over the full range of "degrees of cavitation", but at only one throat velocity. These data resulted in void fraction contours as shown, e.g., in Figure 7 in relation to the venturi wall and damage test specimen position (actually test specimens were not in place during these tests).

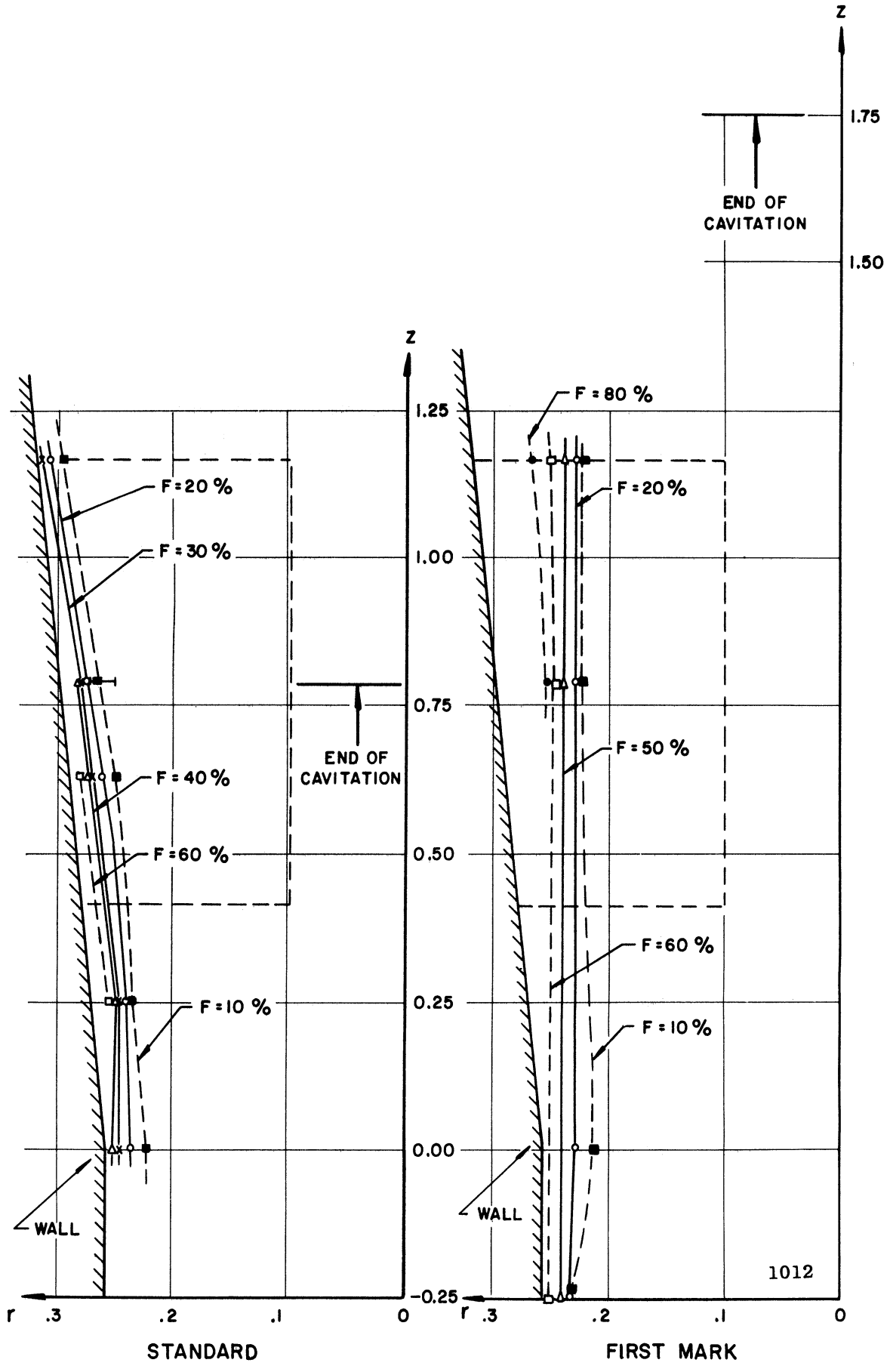

Fi Figure 7. Void Fraction Profiles for Standard and First Mark Cavitation Conditions.

A new set of measurements [2] has been made of mean density, in a plane which includes the venturi centerline, as a function of axial position, again for the various "degrees of cavitation" of interest and including two throat velocities. For these tests the damage specimens were in place. Other than attaining additional basic data on the cavitating flow phenomenon, the purpose of the tests was to develop a technique for the determination of the extent of the cavitating region in non-transparent venturis necessary for high-temperature tests.

For these latter tests, no radial traverses were necessary. Rather the source-detector assembly was moved axially along the venturi centerline, starting from a position 1/4 inch upstream of the cylindrical throat exit (Figure 2) and proceeding in seven steps to a position 1-3/4 inches downstream from the throat exit. At all these positions count-rate was measured for both cavitating and non-cavitating conditions.* In addition back-ground counts were made (with and without the pump operating to insure that the pump motor was not affecting the detection equipment). Typical resultant count-rate profiles, corrected for background, are shown in Figures 8 and 9.

V THEORETICAL ANALYSIS AND DATA REDUCTION

The method for computing local density (or void fraction) from the count-rate traverses was summarized in a previous paper[1] and explained in greater detail in a project report of which that paper is a summary. Some of the salient features of the analytical procedure will now be considered.

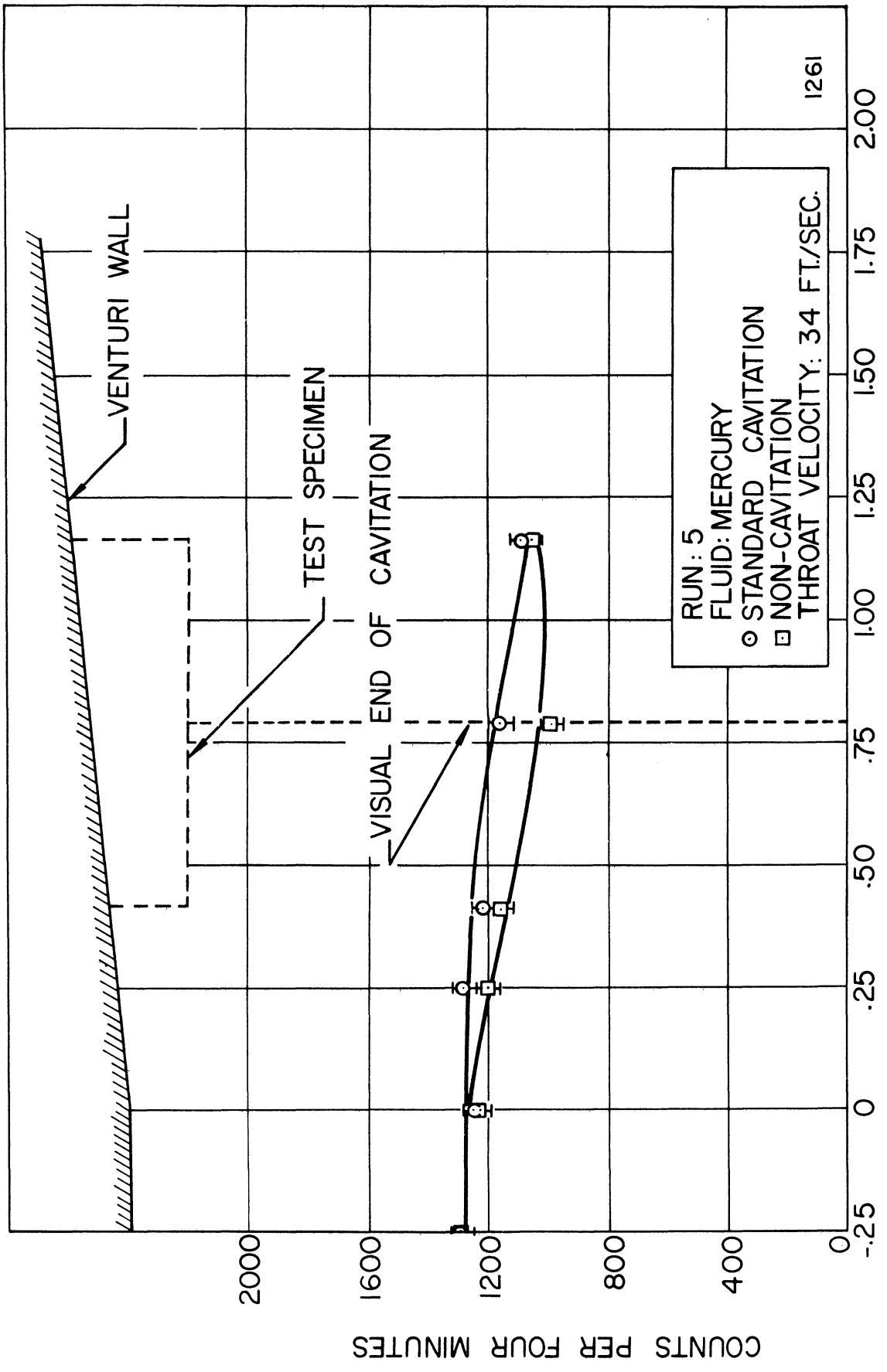

Figure 8. Count-rate vs. Axial Position for Standard Cavitation at 34 ft./sec. Throat Velocity.

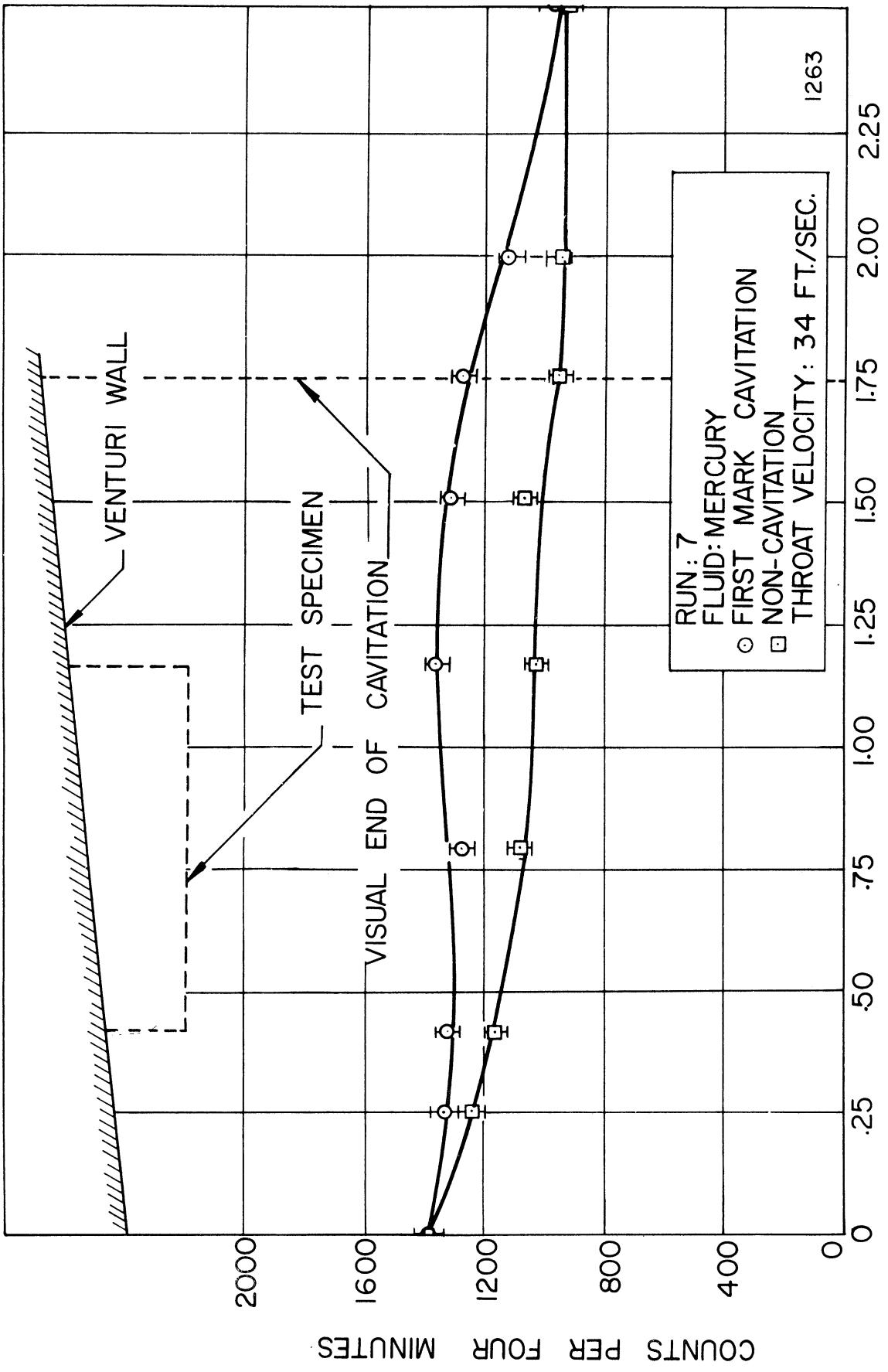

Figure 9. Count-rate vs. Axial Position for First Mark Cavitation at 34ft./sec. Throat Velocity.

On physical grounds it is clear that if the flow is axially-symmetric as assumed, then a single radial traverse must be sufficient to determine local density. Additional traverses cannot provide new information as there is no preferred direction. This is indeed the case.

The determination of mean density for a plane (or thin slab) which includes the gamma-ray beam (Figure 10) is straight-forward provided the dimensions of the system and the absorption coefficient of the liquid (mercury in this case) for the photon energy involved are known. To simplify the determination of a suitable absorption coefficient, only a small energy increment around the photopeak was observed. As shown in the previous paper,[1] the relation for the determination of such a mean density can be arranged so that the absorption coefficient of the container material is not involved. However, it is then necessary to obtain count-rate data for both the case when the test section is filled with liquid only, i.e., no cavitation, and also for the cavitation condition to be observed.

Assuming that the density in the annulus between r and $r + \Delta r$, for sufficiently small Δr, is constant, then an integral relation can be found between this density $\rho(r)$ and the density $\rho(x)$ in a slab of thickness Δx (Figure 10), and the integration performed. $\rho(r)$ can then be determined for the outermost annulus from the count-rate data for the outermost vertical slab. Moving toward the center and using the results from the outer annulus and those from the slab adjacent, toward the center, it becomes possible to determine the mean density of the next inner annulus.

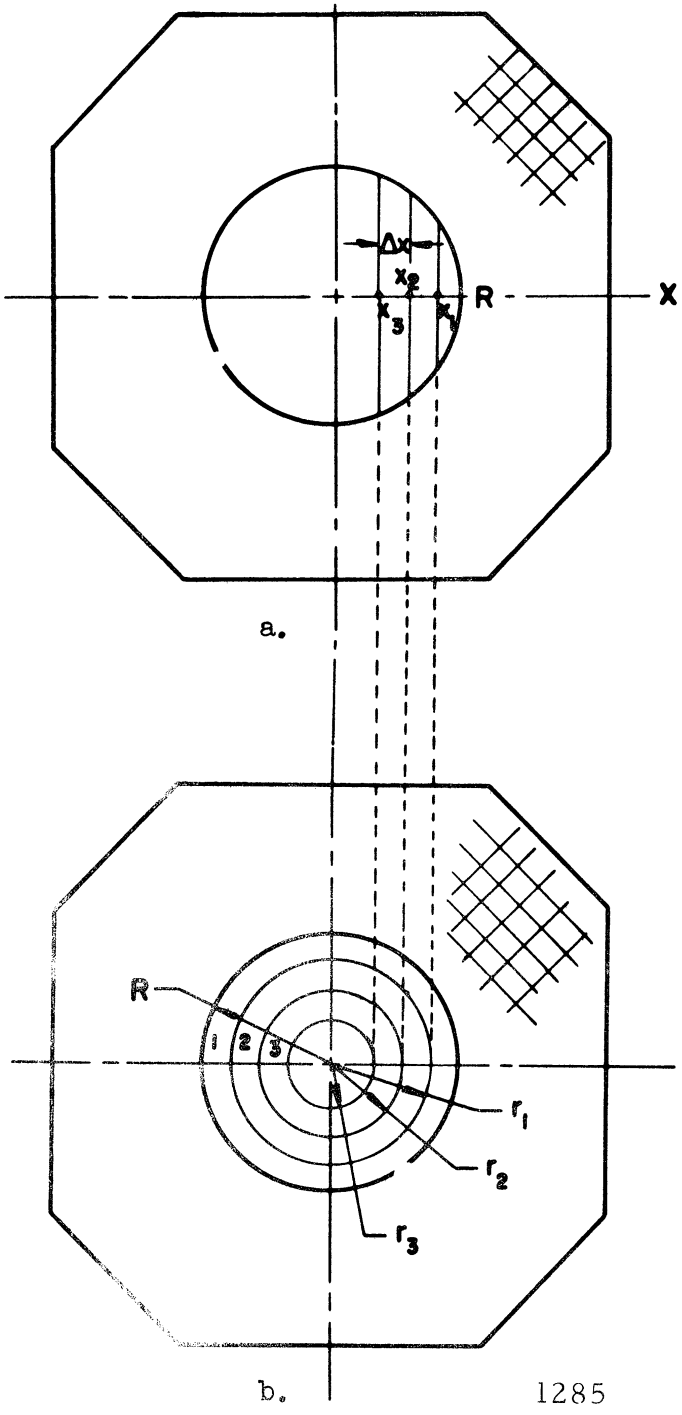

Figure 10. Calculation of $\rho(r)$ from $\rho(x)$.

The process may be continued, moving toward the center until the entire cylinder has been covered. It is of course not necessary that the increments considered in the calculation be the same as those actually used for data-taking, which merely serve to establish a smooth curve of count-rate vs. radius, which can then be incremented in any convenient manner. Since the calculation has been programmed for an IBM 709 computer, it becomes desirable for improved accuracy to use a much finer increment in the calculation than in the experiment, and this has been done.

For the determination of mean density only in a plane including the centerline as a function of axial position, as was done for the second set of experiments herein described, only the first portion of the above calculation is necessary.

A different method[4] for computing local density in an axially-symmetric flow has recently come to the attention of the authors. The void fraction or density radial profile is assumed to be in the form of a power series and the coefficients thereof determined from the experimental data for slabs similar to those mentioned in the previous calculation. The accuracy of the mehtod depends on the number of experimental points used, which is equal to the number of coefficients assumed in the power series.

VI DISCUSSION OF RESULTS

A Local Density Measurements

The results from the earlier local void fraction measurements have already been published.[1] They are best shown in the form of void fraction contours, a typical case of which has already been discussed

(Figure 7). Results of this type were obtained for the degrees of cavitation denoted "Visible Initiation", "Cavitation to Nose", "Standard Cavitation", and "First Mark Cavitation" (see Figure 2 for further definition of these conditions). In all cases the fluid was mercury, and the throat velocity approximately 34 feet per second. These results represent basic data relative to the cavitation flow regimes, which are of particular interest with respect to the damage tests.

B Centerline Plane Mean Density Measurements

Typical count-rate axial profiles for the centerline plane mean density tests have been discussed in an earlier section (Figures 8 and 9). Examination of these curves shows that the cavitating count-rate is consistently higher for all cavitation degrees, starting from approximately the throat discharge and continuing to well beyond the visually apparent end of the cavitating region. The curves shown are for "Standard Cavitation" and "First Mark Cavitation", both at 34 feet per second throat velocity; however, curves are also available[2] at this velocity for the other cavitation degrees of interest, and in two cases also for 48 feet per second.

Computation of mean centerline plane density from the count-rate data was accomplished as already described. The resultant densities were normalized by dividing by liquid mercury density and then plotted as a function of axial position (Figures 11 - 17). The curves include all the cavitation degrees mentioned in connection with the local density measurements as well as "Cavitation to Back", all at 34 feet per second throat velocity. In addition profiles are shown for 48 feet per second and compared with the lower velocity data for "Cavitation to Nose" and "Standard Cavitation".

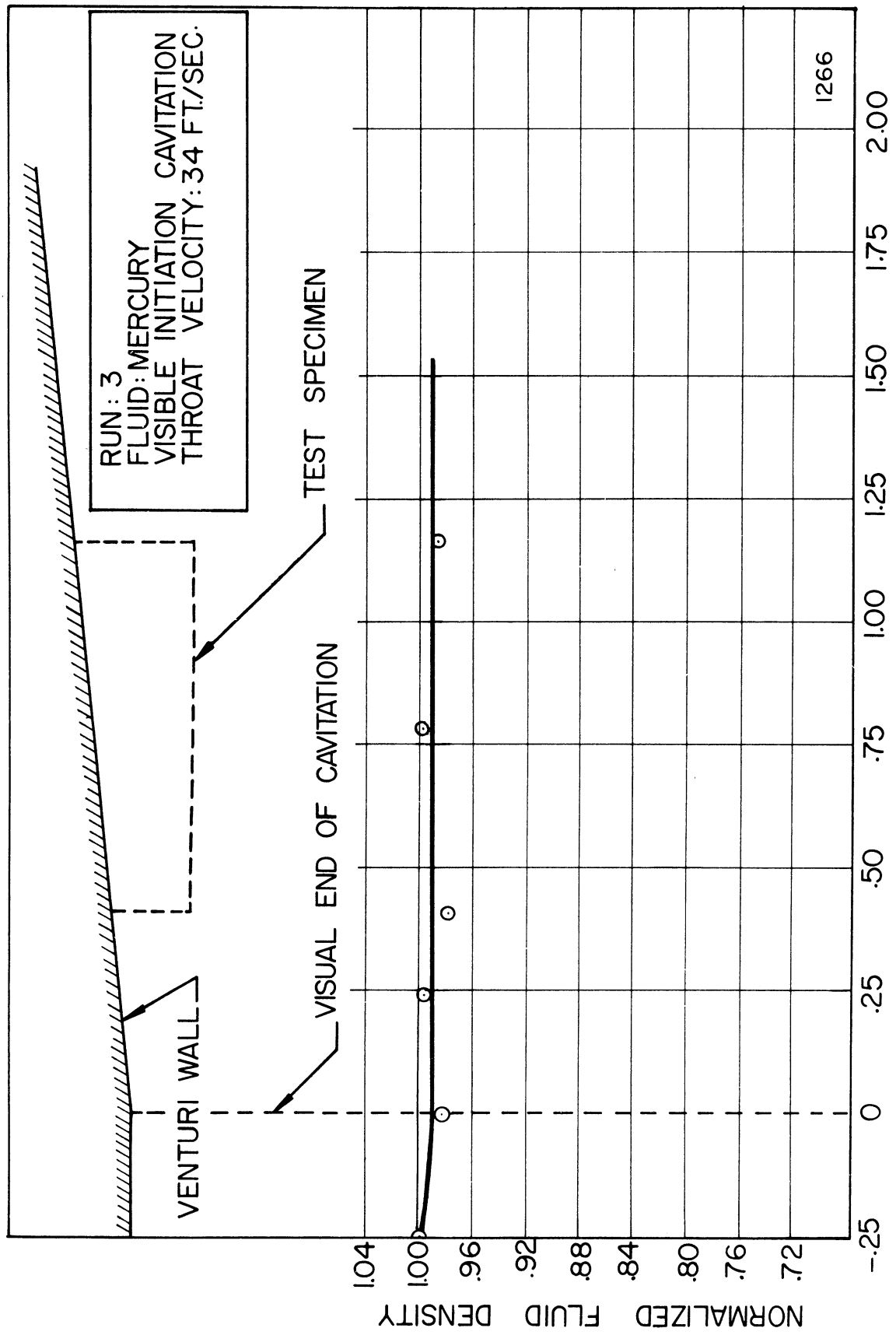

Figure 11. Normalized Fluid Density vs. Axial Position for Visible Initiation at 34 ft./sec. Throat Velocity.

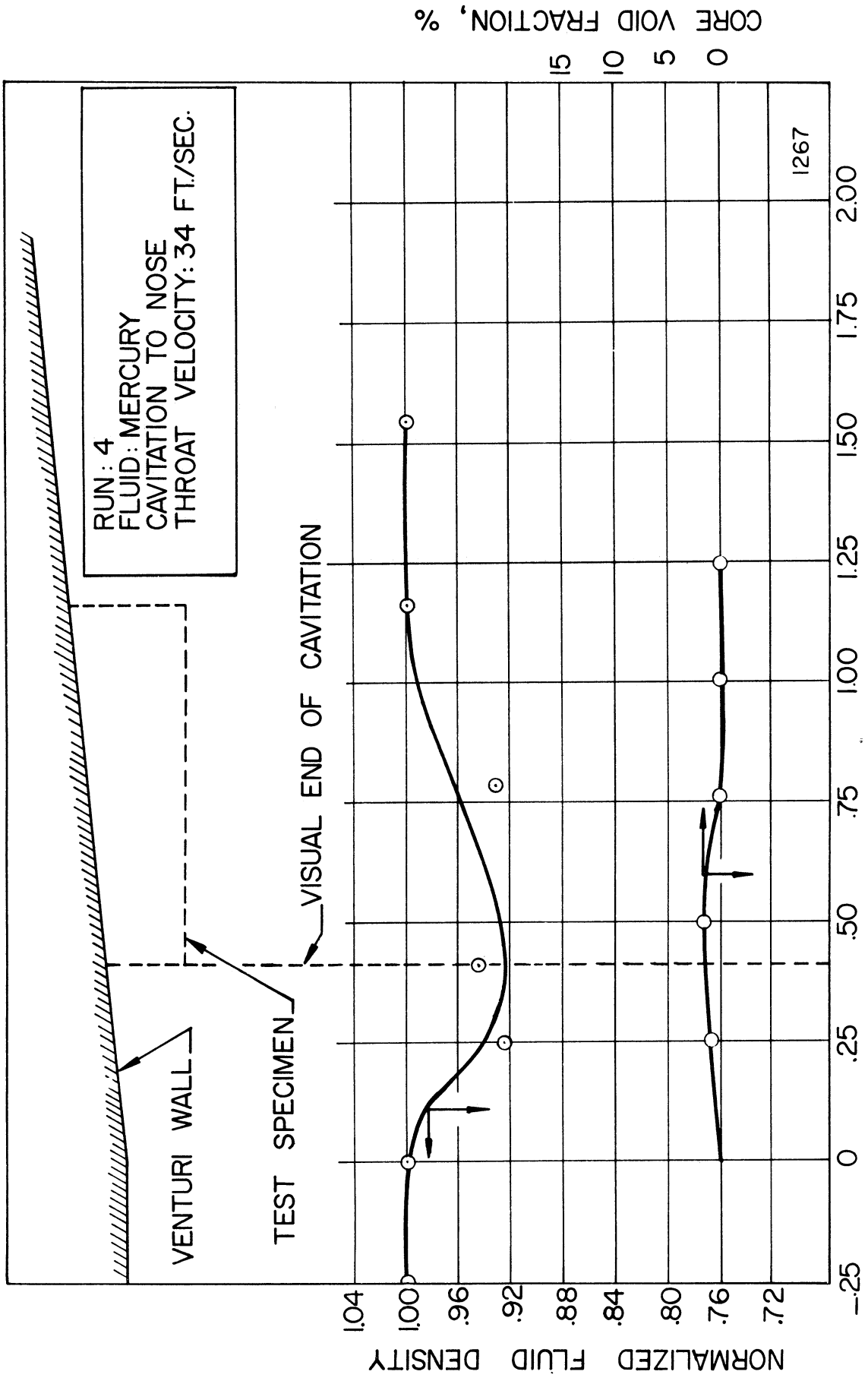

Figure 12. Normalized Fluid Density and Core Void Fraction vs. Axial Position for Cavitation to Nose at 34 ft./sec. Throat Velocity.

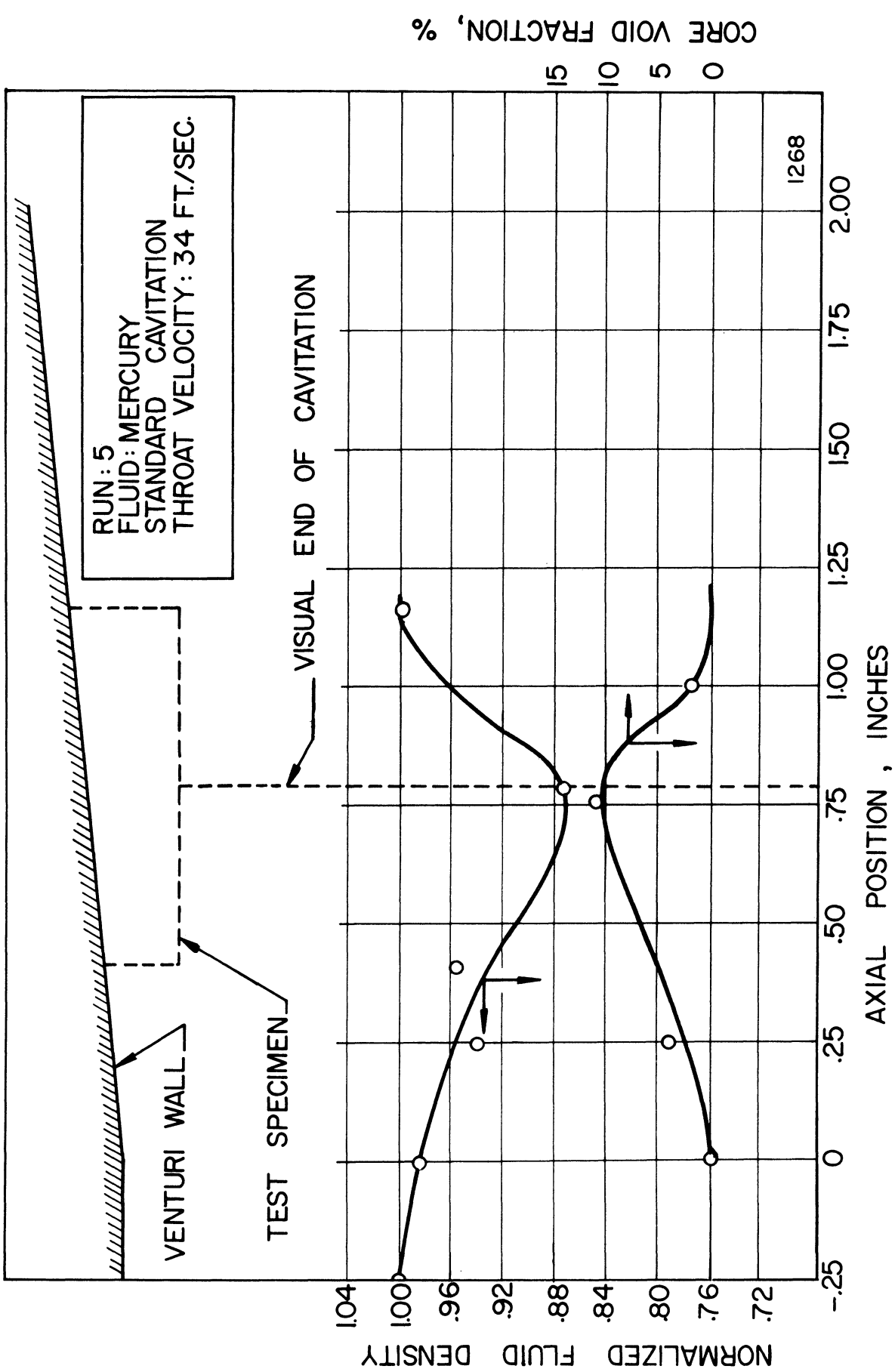

Figure 13. Normalized Fluid Density and Core Void Fraction vs. Axial Position for Standard Cavitation at 34 ft./sec. Throat Velocity.

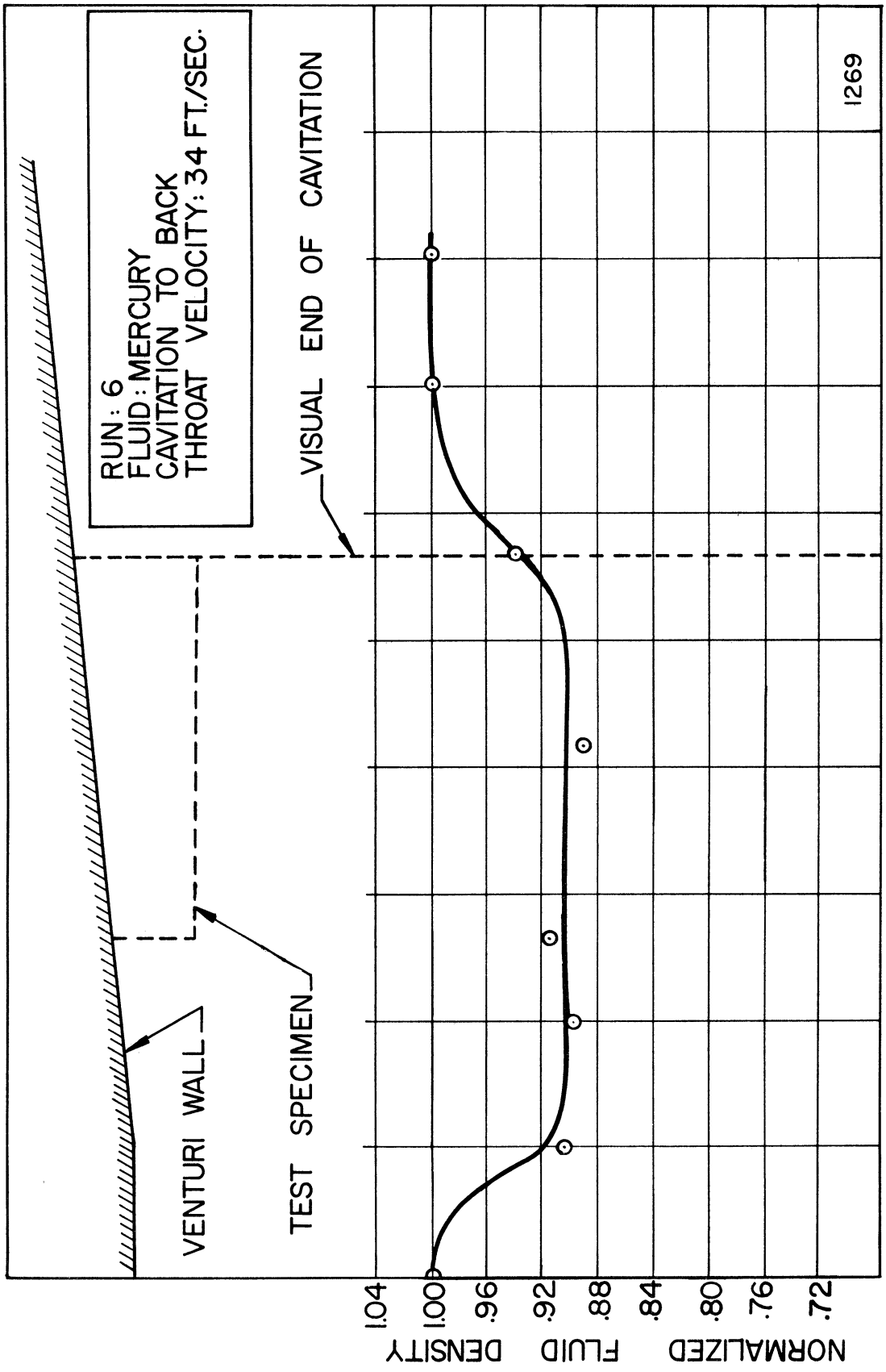

Figure 14. Normalized Fluid Density vs. Axial Position for Cavitation to Back at 34 ft./sec. Throat Velocity.

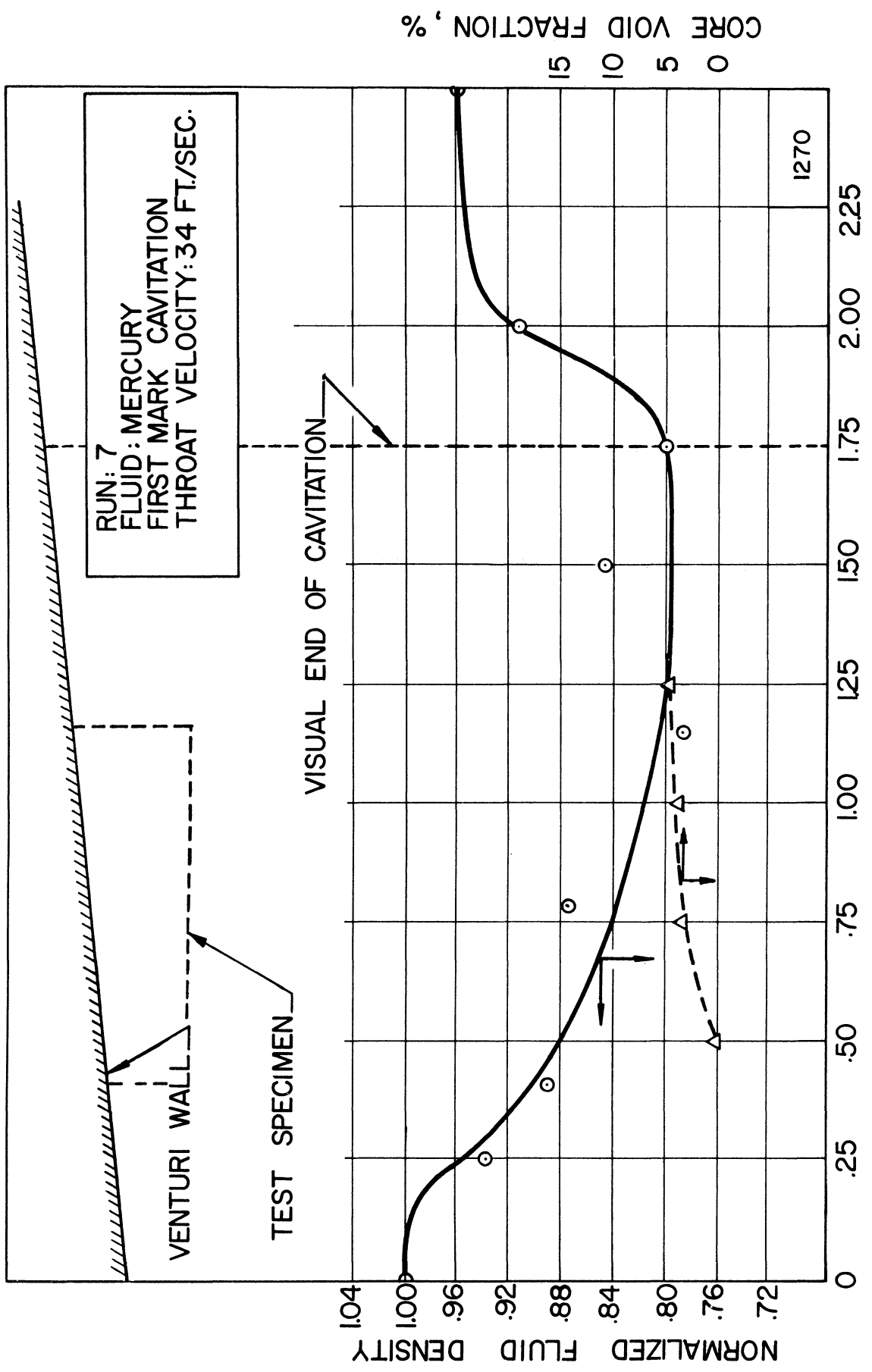

Figure 15. Normalized Fluid Density and Core Void Fraction vs. Axial Position for First Mark Cavitation at 34 ft./sec. Throat Velocity.

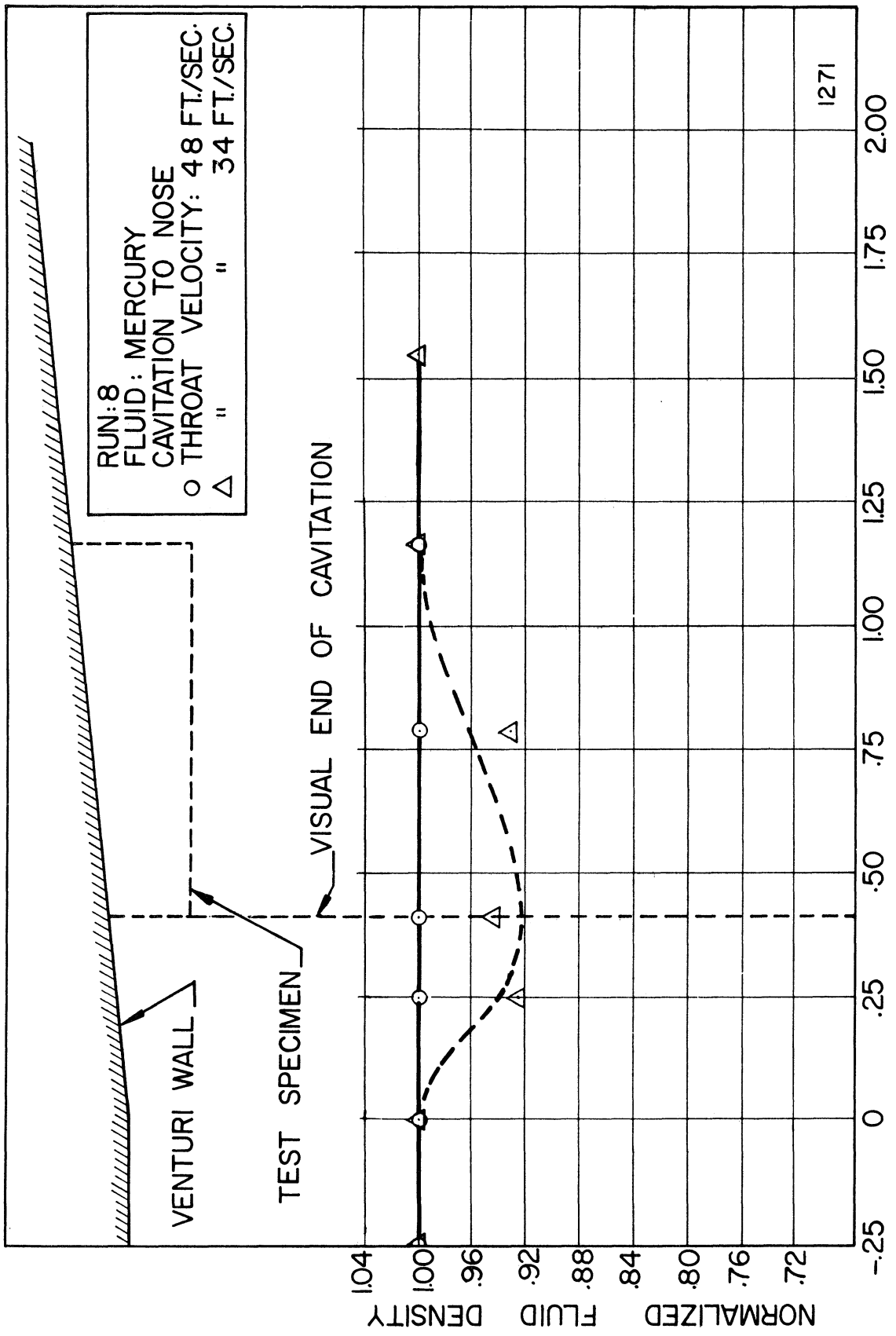

Figure 16. Normalized Fluid Density vs. Axial Position for Cavitation to Nose at 48 and 34 ft./sec. Throat Velocities.

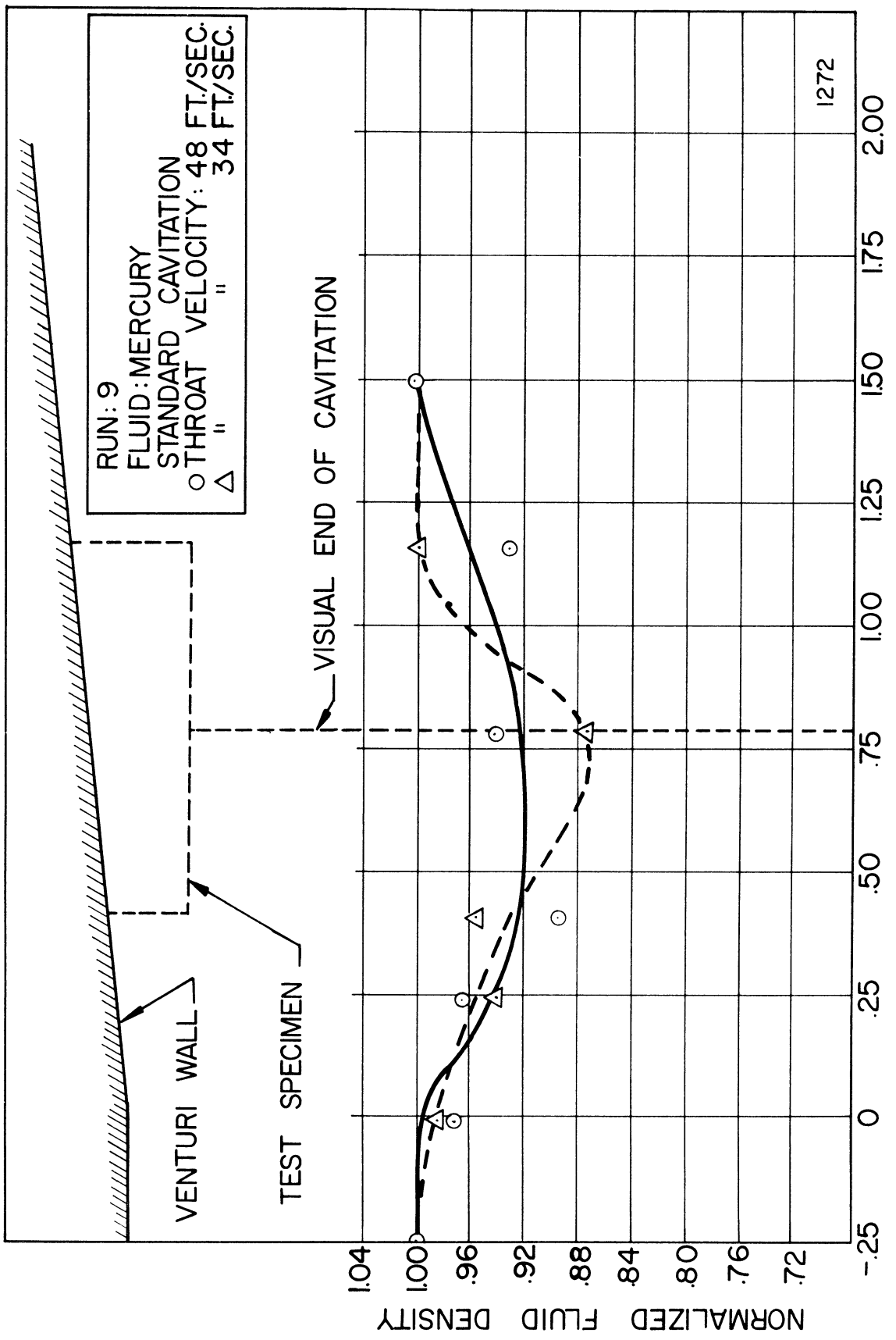

Figure 17. Normalized Fluid Density vs. Axial Position for Standard Cavitation at 48 and 34 ft./sec. Throat Velocities.

An examination of these density profiles discloses the following significant results.

1) The data are generally consistent with the local density measurements previously described (Figure 7) in tnat the significant density reductions start approximately at throat discharge and persist through and well beyond the visually determined point of cavitation termination.

2) Mean centerline density profiles are generally sufficient to establish the cavitation condition for degrees other than initiation (for which the cavitating region is too small for determination in this manner).

3) The positions of maximum density reduction generally correlate well with the visual settings, which correspond approximately to the start of the rise in the density profile. (The precision of visual setting is estimated to be only about $\pm$ 0.10 inches).

4) The decrease in density in the cavitating region is less for higher throat velocity (Figures 16 and 17), for a given cavitation degree as determined by visual setting.** An apparently similar effect has been noted in tests in water wherein the transparency of the cavitating region has been observed to be greater for higher throat velocity and the same cavitation degree. However, an opposite trend has also been noted in previous measurements of "venturi loss coefficient" wherein it was found that the normalized pressure loss for a given visually determined degree of cavitation was greater at high velocity.[3,5]

C Central Jet Axial Density Profiles

It has been established by various methods throughout the present investigation, including localized void fraction measurements,[1] velocity probe measurements,[1] and visual appearance that the flow pattern in the cavitating region of the venturi very generally comprises a central jet which is substantially liquid, has a diameter approximately equal to that of the throat, and a velocity about equal to throat velocity. The central jet is surrounded by a region of substantial void fraction, generally increasing toward the wall (Figure 7, e.g.). However, the accuracy of localized void fraction measurements[1] was not sufficient to measure the void fraction of the central core, beyond ascertaining that it was less than about 10% (Figure 7).

By comparison of the present axial profiles (Figures 11 - 17) with those from the localized measurements,[1] it is possible to compute the mean density of the central fluid jet within the 10% void fraction contour as a function of axial position. Such a calculation supplies new basic data of interest, as well as checking the consistency between the present data and those of the earlier investigation.[1] The required relations are derived in the appendix.

The results, in those cases where direct comparison was possible, are shown by the lower curves in Figures 12, 13, and 15. The maximum void fraction (minimum density) for the central core approximately coincides with the visually determined termination point, and hence the minimum density for the entire centerline plane. Since the void fraction is generally less than 5% and approaches 10% only in one case (Figure 13), it

is apparent that the two sets of measurements are consistent as far as can be determined, and that the central jet is indeed composed almost entirely of liquid.

VII CONCLUSIONS

A method using a gamma-ray densitometer has been developed for obtaining precise measurements of local density (or void fraction) in an axially-symmetric two-phase flow, or of mean density in the centerline (or a parallel) plane. The method has been applied successfully to a cavitating mercury venturi, and various basic measurements of the flow regime obtained. These are listed in the paper. The technique can of course be adopted for use with low-density fluids as water, alkali liquid metals, etc., but a softer radiation source would then be required.

VIII APPENDIX

Central Jet Axial Density Profile Determination

Reference 1 presents void fraction contours for various cavitation conditions as sketched below:

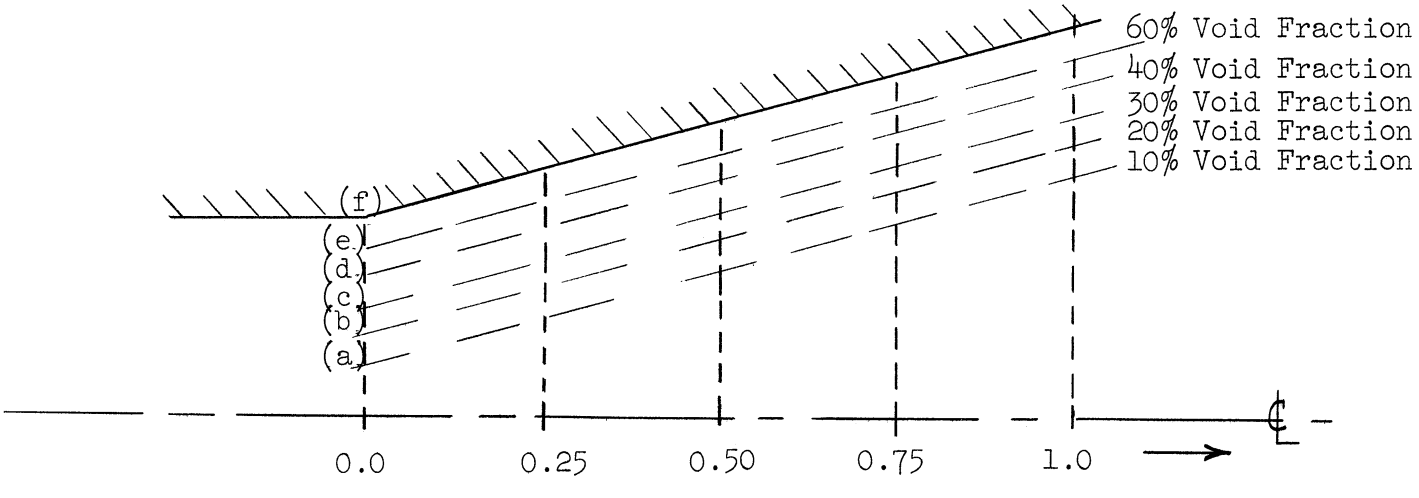

Figure 18. Void Fraction Contour Schematic.

Consider a vertical fluid column of unit cross-sectional area, passing through the center line at any given axial position. Divide this column into segments each extending between adjacent void fraction contours (Figure 18).

Then the total mass in such a fluid column is:

$$\Delta r_{o-a}\,\rho_{o,a} + \Delta r_{a-b}\,\bar{\rho}_{a,b} - - - - - + \Delta r_{e-f}\,\bar{\rho}_{e,f} \qquad (1)$$

$$= \Delta r_{o-a}\,(1 - \overline{V.F.}_{o,a})\rho_L + - - - - + \Delta r_{e-f}(1 - \overline{V.F.}_{e,f})\rho_L \qquad (2)$$

$$= \bar{\rho} r_f$$

$$\text{Thus } \bar{\rho}/\rho_L = \frac{\Delta r_{o-a}(1-\overline{V.F.}_{o-a} - - - + \Delta r_{e-f}(1-\overline{V.F.}_{e,f})}{r_f} \qquad (3)$$

In the right-hand side of Equation (3), all quantities are measured[5] except for $\overline{V.F.}_{o-a}$, which is stated to be less than 10%. The left-hand side is known from the data of the present report.

Hence Equation (3) may be solved for $V.F._{o-a}$ and it is these values which are plotted in Figures 12, 13, and 15.

Appendix Nomenclature:

Δr_{ij} = Radial increment between radius r_i and r_j over which the void fraction changes by about 10%.

$\bar{\rho}_{ij}$ = Average fluid density in the annular ring formed by r_i and r_j, or also the average density in the portion of the vertical column of unit cross section area between r_i and r_j.

$\overline{V.F.}_{ij}$ = Average void fraction in annular ring, between r_i and r_j.

ACKNOWLEDGMENTS

Financial support for the overall project of which this work was a part was furnished by a NASA grant. Much of the electronic instrumentation was lent by the Michigan Memorial Phoenix Project and the Nuclear Engineering Department of The University of Michigan.

REFERENCES AND FOOTNOTES

1. W. Smith, G. L. Atkinson, and F. G. Hammitt, ASME Paper No. 63-AHGT-19, to be published in Trans. ASME, J. Basic Engr.; also in expanded form as ORA Project 03424, Tech. Rept. No. 7, The University of Michigan, Sept., 1962.

2. I. E. B. Lauchlan, F. G. Hammitt, R. D. Ivany, M. J. Robinson, W. Smith, "Determination of Cavitation Conditions from Density Profiles of Mercury in a Venturi" ORA Project 03424 Tech. Rept. No. 11, The University of Michigan, Oct., 1963.

3. F. G. Hammitt, Trans. ASME, Series D, J. Basic Engr., 85, 1 - 12 (1963).

4. J. A. Vogrin, Jr., "An Experimental Investigation of Two-Phase, Two-Component Flow in a Horizontal, Converging — Diverging Nozzle", ANL-6754 (1963).

5. F. G. Hammitt, R. D. Ivany, V. F. Cramer, M. J. Robinson, "Observations of Cavitation Scale and Thermodynamic Effects in Stationary and Rotating Components with Water and Mercury", ORA Project 03424 Tech. Rept. No. 6, The University of Michigan, Sept., 1962.

* A separate non-cavitating profile was made for each cavitating run to avoid errors due to drift of the electronics over long time periods.

** The data for high velocity are less consistent than for low. It is felt that this may result from increased system vibration and the increased difficulty of maintaining steady state.

LIST OF FIGURE TITLES

1 Overall loop layout.

2 Cross Section of cavitating venturi test section showing locations of metal wear specimens and locations of the cavitation termination for various degrees of cavitation.

3 Cross section of densitometer.

4 Densitometer positioned at venturi.

5 Block diagram of electronic equipment.

6 Determination of venturi centerline by densitometer method, assuming axial symmetry.

7 Void fraction profiles for Standard and First Mark Cavitation conditions.

8 Count-rate vs. axial position for Standard Cavitation at 34 ft./sec. throat velocity.

9 Count-rate vs. axial position for First Mark Cavitation at 34 ft./sec. throat velocity.

10 Calculation of $\rho(r)$ from $\rho(x)$.

11 Normalized fluid density vs. axial position for Visible Initiation at 34 ft./sec. throat velocity.

12 Normalized fluid density and core void fraction vs. axial position for Cavitation to Nose at 34 ft./sec. throat velocity.

13 Normalized fluid density and core void fraction vs. axial position for Standard Cavitation at 34 ft./sec. throat velocity.

14 Normalized fluid density vs. axial position for Cavitation to Back at 34 ft./sec. throat velocity.

15 Normalized fluid density and core void fraction vs. axial position for First Mark Cavitation at 34 ft./sec. throat velocity.

16 Normalized fluid density vs. axial position for Cavitation to Nose at 48 and 34 ft./sec. throat velocities.

17 Normalized fluid density vs. axial position for Standard Cavitation at 48 and 34 ft./sec. throat velocities.

18 Void fraction contour schematic.